Coverage-dependent anisotropy of the NTCDA/Ag(111) interface state dispersion

L. Eschmann,[1,*] A. Sabitova,[2,3,4] R. Temirov,[2,3,5] F. S. Tautz,[2,3,4] P. Krüger,[1] and M. Rohlfing[1]

[1]*Institut für Festkörpertheorie, Westfälische Wilhelms-Universität Münster, 48149 Münster, Germany*

[2]*Peter Grünberg Institut (PGI-3), Forschungszentrum Jülich, 52425 Jülich, Germany*

[3]*Jülich Aachen Research Alliance, Fundamentals of Future Information Technology, 52425 Jülich, Germany*

[4]*Experimental Physics IV A, RWTH Aachen University, Otto-Blumenthal-Straße, 52074 Aachen, Germany*

[5]*II. Physikalisches Institut, Universität zu Köln, Zülpicher Straße 77, 50937 Köln, Germany*

(Received 1 July 2019; published 24 September 2019)

We employ density functional theory (DFT) to analyze the dispersion of the electronic state that exists at the commensurate interface between a monolayer of 1,4,5,8-naphthalene-tetracarboxylic acid dianhydride (NTCDA) and the Ag(111) surface. First, we present and verify a hydrogen-termination approach which allows a meaningful DFT description of the interface state with relatively thin silver slabs. Complemented with a projection technique which maps the interface electronic structure onto the original Ag(111) Shockley state, the DFT calculations enable us to analyze the evolution of the dispersion of the NTCDA/Ag(111) interface state when changing of the molecular coverage. Our calculations yield a difference between the interface state energy and the Shockley state energy that scales linearly with coverage. Furthermore, they predict a pronounced anisotropy of the dispersion of the interface state at long wavelengths which also depends linearly on the molecular coverage. The dispersion anisotropy is fully confirmed by our Fourier transform (FT) scanning tunneling spectroscopy (STS) experiments performed on a relaxed phase NTCDA/Ag(111) monolayer. Using feature detection STS (FD-STS), we moreover measure a band gap in the interface state band structure at the Brillouin zone boundary which indicates Bragg scattering of the interface state electrons in the periodic potential of the molecular layer. We thus observe an influence of the molecular layer on the interface state both at long (DFT, STS) and short wavelengths (STS).

DOI: 10.1103/PhysRevB.100.125155

I. INTRODUCTION

The adsorption of π-conjugated organic molecules on metallic substrates often produces peculiar electronic structures that result from interactions between energetically discrete and localized molecular orbitals on the one hand and continuous and delocalized states of the metal on the other. These interactions may lead to energy shifts and hybridization of molecular orbitals [1–3], charge transfer [4–7], as well as the Kondo effect [8–10]. The two-dimensional (2D), highly dispersive interface states that often appear at the interfaces between an ordered monolayer of π-conjugated organic molecules and a metal surface [11–19] are particularly noteworthy. Although interface states at metal surfaces were initially discussed for adsorption of noble gases or monolayers of NaCl [20,21], the first instance of such a state at an ordered monolayer of π-conjugated organic molecules was discovered at the interface between a commensurate 3,4,9,10-perylene-tetracarboxylic acid dianhydride (PTCDA) monolayer and the Ag(111) surface [11].

Since their original discovery, the nature of these strongly dispersive metal-organic interface states has been debated. Initially proposed to be *hybrid* metal-molecule states that originate from a metal-mediated coupling between neighboring unoccupied molecular orbitals [11], they have later been attributed to a Shockley state *of the metal* that is shifted up in energy due to the modification of the surface barrier induced by the adsorption of the organic monolayer [13]. Following the latter view, it was suggested that the structure of both the molecular species in question and its monolayer arrangement influence the properties of the interface state exclusively by defining some effective vertical adsorption height; a one-dimensional (1D) potential in the vertical direction should thus be sufficient to model the interface state [22]. Despite its success in describing the interface state onset energies of many systems, it is evident that this model must remain incomplete, as by construction it neglects the influence of adsorption coverage as well as lateral structure of the molecular layer on the electronic structure of the interface state at finite wavelengths, e.g., its dispersion. In fact, recent evidence shows that such an influence does indeed exist: in feature detection scanning tunneling spectroscopy (FD-STS) band gaps have been observed at the Brillouin zone (BZ) boundaries of the molecular superstructure [23]. These band gaps prove that the interface state is scattered by the laterally corrugated potential of the molecular layer.

In this paper we show that the influence of the molecular layer on the properties of the interface state is not restricted to wave vectors close to the BZ boundary where scattering is expected to be strong even in a weak periodic potential. On the contrary, we demonstrate that this influence is also present at long wavelengths where the interface state essentially behaves as a free-electron state with parabolic dispersion.

*l.eschmann@uni-muenster.de

Specifically, we show by density functional theory (DFT) and scanning tunneling spectroscopy (STS) that a molecular layer of 1,4,5,8-naphthalene-tetracarboxylic acid dianhydride (NTCDA) on Ag(111) creates an anisotropy in the free-electron interface state band structure. Thus, the response of electrons in the interface state to an electric field depends on the direction of the latter with respect to the molecular layer. This anisotropy becomes increasingly pronounced as the molecular coverage rises; it reaches its maximum for the relaxed monolayer phase [24] of NTCDA.

In our DFT calculations we use the standard approach where a sufficiently thick slab of silver, periodically spaced in the vertical direction, is used to describe the substrate. From previous theoretical work [14,16] it is known that the converged description of both the Shockley and the interface states is only possible for a rather large number of atomic silver layers, which obviously comes at considerable computational costs. In fact, the large number of substrate layers prohibits the investigation of low molecular coverages because the latter require large surface supercells in addition to the many substrate layers. To make such calculations feasible, we therefore must find a way to reduce the computational costs for calculating the interface state.

To this end, we have developed a scheme that allows the systematic analysis of the interface electronic structure even in the case of very large surface supercells. We first show that converged computations of the Ag(111) Shockley state need a large number of silver layers mainly in order to suppress the interaction between the identical surface states located at the top and bottom surfaces of the slab. We circumvent the need for a large number of layers by terminating the bottom of the slab with atomic hydrogen. This shifts the energy of the bottom Shockley state up in energy and thus hinders its interaction with the top Shockley state. We have adopted this approach from DFT studies of semiconductors, where the passivation of one of the surfaces with hydrogen is commonly used to inhibit the interaction between the top and bottom surface states [25].

A second methodological problem that we address here is the backfolding of the band structure. For large surface supercells, backfolding produces a large number of bands in the BZ of the supercell, which makes the analysis of the band structure very challenging. For example, for NTCDA/Ag(111) we encounter up to 49 times as many bands in the supercell BZ as in the primitive BZ of Ag(111). Previously, several unfolding procedures have been proposed that determine the primitive spectral function or band structure for both localized and plane-wave basis sets [26,27]. Although these techniques are able to reveal the dispersion of the interface state in the primitive cell [18], the weights that are obtained in this way merely measure the Bloch periodicity of the states; this is not very selective and may in fact prohibit a quantitative examination of their Shockley-type character. Therefore, we have developed a projection technique which maps the states of the *adsorbate system* onto the original Shockley state (or other states) of the *pure surface* (i.e., without adsorbates) in its primitive unit cell. Not only does this allow us to recover the dispersion of the interface state and to evaluate its effective mass quantitatively, it also objectively reveals the degree to which any state in the band structure has a Shockley character.

On the basis of these two methodological developments, a detailed, systematic, and quantitative theoretical investigation of the interface state band structure, in particular with respect to its coverage dependence, its anisotropic dispersion, and a possible formation of band gaps [23] becomes possible. Most notably, the DFT data for the NTCDA/Ag(111) system that are presented below show that the dispersion of the interface state is anisotropic and that the anisotropy rises with increasing coverage of molecules. Our experimental STS study of the relaxed monolayer reveals an anisotropy of the interface state dispersion that agrees with our theoretical prediction.

II. THEORETICAL APPROACH

A. Density functional theory

In this work, we perform calculations within density functional theory (DFT) using the SIESTA code [28,29] for geometrical optimization, while band structure calculations have been carried out with a code developed in our group [30–32]. Both codes work within a localized basis set.

SIESTA uses a basis representation of numerical orbitals [33,34] and implements norm-conserving Troullier-Martins pseudopotentials [35]. Since the common exchange-correlation functionals are not suited to describe the adsorption geometry of metal-organic interfaces, our geometrical optimization takes the long-range behavior of the van der Waals (vdW) interaction explicitly into account. This is achieved by using the combined nonempirical DFT + $\mathrm{vdW}^{\mathrm{surf}}$ [36] and Lifshitz-Zaremba-Kohn method proposed by Ruiz *et al.* [37]. It provides an energy correction term to the generalized gradient approximation functional by Perdew, Burke, and Ernzerhof (PBE) [38]. The C_6 coefficients are taken from Ref. [37] for bulk Ag and from Ref. [36] for the C, O, and H atoms. They are used without Hirshfeld partitioning. The determination of the interaction coefficients is based on the polarizabilities from Ref. [39].

The Ag(111) surface is described by periodically repeated slabs with at least 20 Å of vacuum between the slabs and the bulk silver lattice constant of 4.062 Å [40]. For the geometrical optimization of adsorbates on Ag(111) we use the SIESTA code, employing a silver slab of three layers, where we keep the position of the silver atoms fixed. We use a double-ζ polarized (DZP) basis [41] with a corresponding energy shift of 0.002 Ry. The real space is defined by a cutoff of 250 Ry. We employ $\vec{k}$ grids with $(6 \times 4 \times 1)$ and $(3 \times 3 \times 1)$ mesh points for the NTCDA monolayer and the noninteracting dilute case (see below), respectively.

The band structure calculations for various numbers of Ag layers (between 3 and 30) were performed with our own code which employs *ab initio* norm-conserving pseudopotentials in the separable Kleinman-Bylander form [42,43]. The basis set is represented by Gaussian orbitals with s, p, d, and s^* symmetry [31,44]. The band structures were obtained using the exchange-correlation functional within the local density approximation (LDA) in the form of Ceperley and Alder with the parametrization of Perdew and Zunger [45,46]. The Fermi energy is converged better than 10 meV with respect to the $\vec{k}$ grid, where the actual grid depends on the respective geometry. We use a real-space mesh density of more than

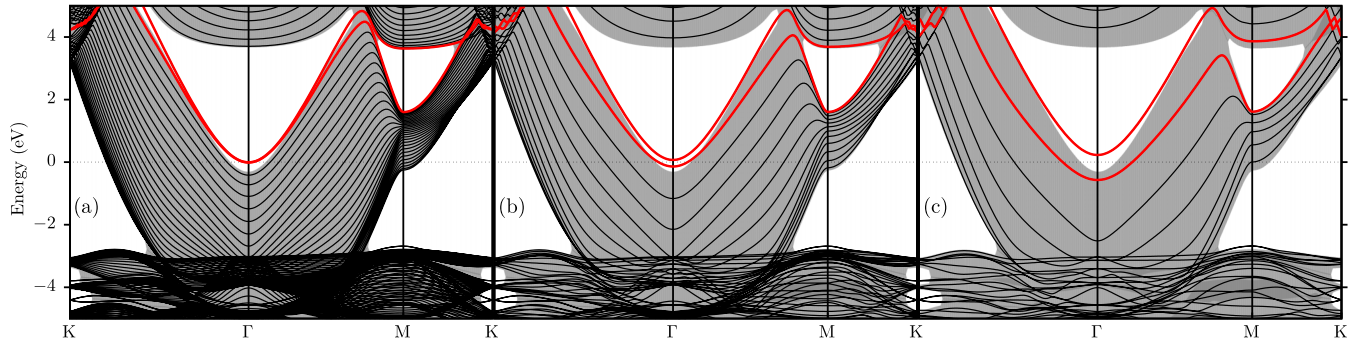

FIG. 1. Band structure of the Ag(111) surface, calculated with DFT. Slab thickness of (a) 30 layers, (b) 12 layers, (c) 6 layers have been used. The parabolic Shockley surface state bands of both slab surfaces are marked in red. The gray area shows the surface-projected band structure of the bulk Ag crystal. Decreasing the number of layers leads to an increased splitting of the Shockley state.

6.6 points per Å for the bare silver surface, which is enlarged to 8 and 13 points per Å for calculations with CO and NTCDA adsorbates, respectively. For a better description of the long-range behavior of the surface and interface states, we place additional orbitals in the vacuum, at the fictitious positions of two further Ag layers. The *details* of these orbitals do have a small influence on the precise energetic position of the Shockley state (in the order of a few meV), but effective masses, splittings between top and bottom surface states, and energy differences between surface and interface states are affected only negligibly. Note that further additional orbitals are placed at the atomic positions of the adsorbate molecules, if applicable, thus leading to slightly different results for the Shockley state energy calculated in the corresponding basis sets in Sec. II B [bare Ag(111)], Sec. III A [CO/Ag(111)], and Sec. III B [NTCDA/Ag(111)].

B. Hydrogen-terminated asymmetric slabs

The Shockley surface state of Ag(111) plays a crucial role in the formation of the NTCDA/Ag(111) interface state, and hence the correct description of the former is vital for the adequacy of our analysis of the latter. Previously, it has been found that a converged description of the Shockley surface state requires a large number of silver layers [14,16]. As we must calculate large surface supercells for the NTCDA/Ag(111) system, which demands a substantial computational effort, we introduce an approach that enables the converged description of the Shockley state, as well as the interface state, while using only a reduced number of atomic layers.

The bare Ag(111) slab calculations were performed using an in-plane (56×56) $\vec{k}_\parallel$ grid. The surface structure of the slab has not been relaxed. The resulting band structures of the DFT calculation for different numbers of layers are shown in Fig. 1. The gray area is the surface-projected band structure resulting from a periodic bulk calculation. It marks all energies occurring for a certain $\vec{k}_\parallel$. For this bulk calculation, the direction perpendicular to the slab surface ($\vec{k}_\perp$) was sampled with 23 grid points. Since the slab has two surfaces, we observe two Shockley states that interact with each other due to their overlap inside the slab (see below). In the band structure obtained with 30 layers, the two Shockley states are almost degenerate with a parabolic dispersion around Γ and an energy at Γ of $E_{\mathrm{SS}} \equiv E_{\mathrm{SS}}^{(30)}(\vec{k} = \Gamma) = -7\,\mathrm{meV}$. Due to the symmetry of the system, both states in the band structure are linear combinations of the top-surface Shockley state and the corresponding state of the bottom. Therefore, they are equally located at both surfaces of the slab. The charge density of one linear combination on one side of the slab is shown in Fig. 2. This state shows the typical Shockley behavior with a slowly decaying exponential envelope function inside the slab and a fast exponential decay in the vacuum outside the surface [22,47,48].

We have also calculated the band structure for thinner slabs. As can be seen in Figs. 1(b) and 1(c) reducing the number of layers M leads to an energy splitting $\Delta E^{(M)} \equiv E_+^{(M)} - E_-^{(M)}$, which was also seen by Zaitsev *et al.* for three, six, and nine layers [14]. This splitting can be understood by considering a two-level system with a Hamiltonian

$$\hat{H}^{(M)}(\vec{k}) = \begin{pmatrix} E_{\mathrm{SS}}^{(M)}(\vec{k}) & V^{(M)} \\ V^{(M)} & E_{\mathrm{SS}}^{(M)}(\vec{k}) \end{pmatrix} \tag{1}$$

$$\Rightarrow E_\pm^{(M)}(\vec{k}) = E_{\mathrm{SS}}^{(M)}(\vec{k}) \pm V^{(M)}, \tag{2}$$

where $E_\pm^{(M)}(\vec{k})$ denote the M-dependent energies of the two linear combinations, respectively. $E_{\mathrm{SS}}^{(M)}(\vec{k})$ denotes the energy

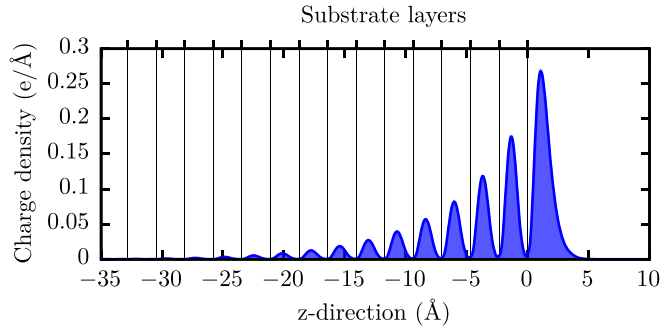

FIG. 2. Line charge density of the Shockley state at $\vec{k}_\parallel = \Gamma$, calculated with DFT for the 30-layer slab. The charge density is integrated over the in-plane coordinates within the unit cell. Vertical lines indicate the substrate layers of the Ag(111) slab. Only one of the two linear combinations of surface states is plotted (see main text). Moreover, the figure shows only one of the similar looking slab surfaces.

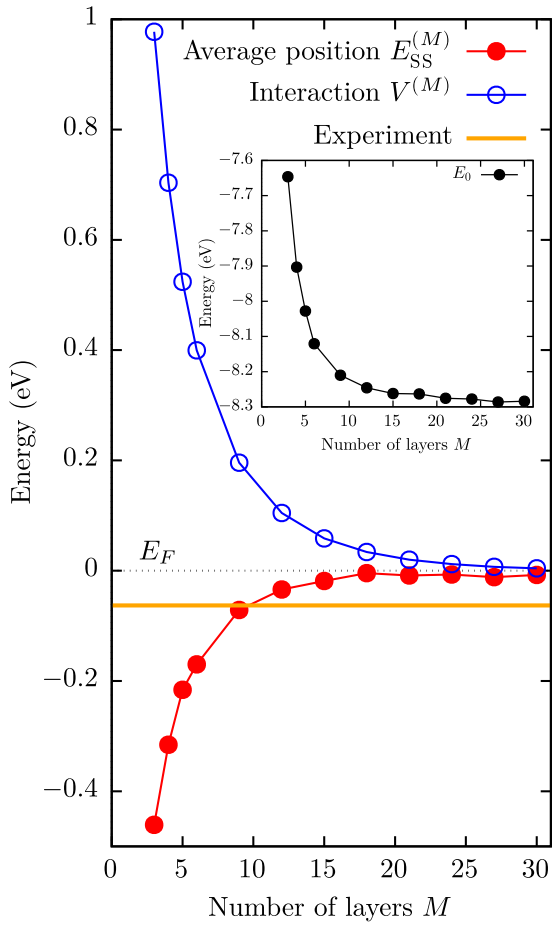

FIG. 3. Properties of the DFT-calculated Shockley surface state as a function of slab thickness. Open blue circles: interaction $V^{(M)}$ between the interacting surface states of both surfaces. Solid red circles: average energetic position $E_{SS}^{(M)}$ relative to the Fermi energy E_F. Solid orange line: experimental value E_{SS} from Ref. [49]. Inset: position of the lowest occupied energy in the system E_0 relative to the Fermi level.

of the original (noninteracting) Shockley state (see next paragraph concerning its dependence on M), which according to Eq. (2) coincides with the average of the two observed energies $E_{\pm}^{(M)}(\vec{k})$. $V^{(M)}$ is interaction between the original Shockley states at the top and bottom surfaces of the slab. The interaction $V^{(M)}$ as a function of slab thickness is shown in Fig. 3. The interaction increases exponentially with decreasing number M of layers. This is a direct consequence of the increasing overlap and interaction of the top and bottom Shockley states. Fitting the DFT results with Eq. (1), we get $V^{(12)} \approx 0.1\,\text{eV}$ for 12 Ag layers, while the interaction increases to $V^{(6)} \approx 0.4\,\text{eV}$ for 6 layers.

Remarkably, Fig. 3 also shows that the average energy $E_{SS}^{(M)}$ decreases with decreasing number of layers. Such changes result from the truncation of each Shockley state at the other surface of the slab (in particular for small M), as well as from the quantization of the parabolic bulk states in the slab of finite thickness. With decreasing number of layers M the number of bulklike states reduces, their energy spacing increases (cf. Fig. 1), and the lowest state E_0 is shifted to higher energy with respect to the Fermi energy. The latter can be seen in the inset of Fig. 3. Like the number of all bulklike states in the band structure, the overall charge occupancy should be proportional to M. However, as these states have parabolic dispersion, the decreasing M yields a lower charge occupancy per bulklike state. The remaining charge therefore increases the occupancy of the surface state and thus its onset $E_{SS}^{(M)}$ appears at lower energies for smaller M. For $M \gtrsim 15$, $E_{SS}^{(M)}$ converges to about $-7\,\text{meV}$, i.e., is located slightly below the Fermi energy. The fact that this converged value deviates from the experimental value of $E_{SS} = (-63 \pm 1)\,\text{meV}$ [49] can be explained with the neglect of surface relaxations as well as general inaccuracies of DFT. Note that in spite of this discrepancy, the energies we obtain from our linear-combination-of-atomic-orbitals (LCAO) approach with 9- and 12-layer slabs, $E_{SS}^{(9)} = -71\,\text{meV}$ and $E_{SS}^{(12)} = -34\,\text{meV}$, agree well with published theoretical results of Tsirkin *et al.* [18] who obtain $E_{SS}^{(10)} = -45\,\text{meV}$ with a plane-wave basis set using a 10-layer slab.

To overcome the interaction between the top and bottom surface states and having Eq. (1) in mind, we place hydrogen atoms on top of the silver atoms at the bottom surface of the slab. The H-Ag distance is chosen to be 2.5 Å. This increases the energy of the bottom surface state by Δ_H, and therefore modifies the Hamiltonian to

$$\begin{pmatrix} E_{SS}^{(M)}(\vec{k}) & V^{(M)} \\ V^{(M)} & E_{SS}^{(M)}(\vec{k}) + \Delta_H \end{pmatrix}. \tag{3}$$

In the present case, hydrogen termination yields a value of $\Delta_H \approx 1.8\,\text{eV}$. If $V^{(M)}$ is small enough, this leads to a near-complete decoupling of the top and bottom eigenstates:

$$E_{\pm}^{(M)}(\vec{k}) = E_{SS}^{(M)}(\vec{k}) + \frac{\Delta_H}{2} \pm \sqrt{\frac{\Delta_H^2}{4} + [V^{(M)}]^2},$$
$$\overset{V^{(M)} \ll \Delta_H}{\approx} \begin{cases} E_{SS}^{(M)}(\vec{k}) + \Delta_H, \\ E_{SS}^{(M)}(\vec{k}). \end{cases} \tag{4}$$

The results for the band structures of asymmetrically hydrogen-terminated six- and nine-layer slabs are shown in Fig. 4. Figure 4(a) shows an overview of the band structure for six layers. Most parts of the band structure are not affected by the hydrogen atoms at the bottom surface of the slab. However, there are some changes compared to Fig. 1(c). For example, between the K and Γ points, and also between K and M, hydrogen-related bands occur outside the surface-projected bulk band structure between 0 and 1 eV. But, the most important change concerns the energy of the Shockley states, as shown in Figs. 4(b) and 4(c) for six- and nine-layer slabs. In both cases, $E_{-}^{(M)}$ is located between the two former states for the symmetric slab and $E_{+}^{(M)}$ is shifted to higher energies by as much as 1.8 eV. We obtain $E_{-}^{(6)} = -169\,\text{meV}$ for six Ag layers and $E_{-}^{(9)} = -54\,\text{meV}$ for nine Ag layers. This agrees well with the averaged energies of $E_{SS}^{(6)} = -170\,\text{meV}$ and $E_{SS}^{(9)} = -71\,\text{meV}$ for the corresponding symmetric slabs.

Figure 5 illustrates the difference in charge density of the surface state between symmetric slabs and hydrogen-terminated asymmetric slabs for $M = 6$. The linear

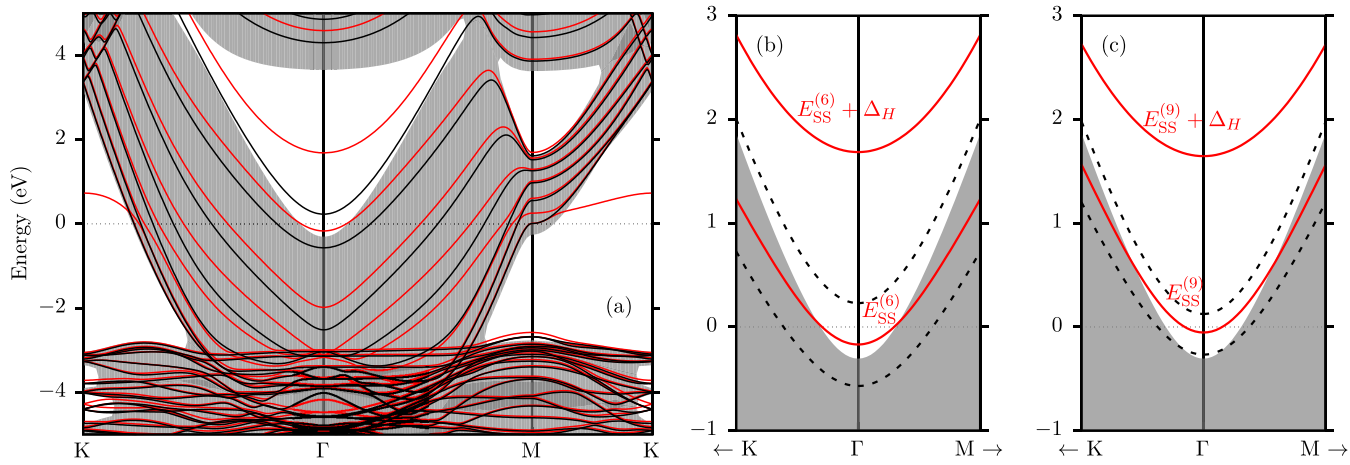

FIG. 4. Band structures of the Ag(111) surface, calculated with DFT using a symmetric slab, compared to calculations for an asymmetric slab that is terminated on the bottom surface with hydrogen. (a) Band structure along the $\vec{k}$-space path shown in Fig. 10, calculated for symmetric (black lines) and asymmetric (red) six-layer slabs. The surface-projected bulk band structure is shown in gray. The Fermi level is set to zero. The black bands are the same data as displayed in Fig. 1(c). (b) Dispersion of the Shockley states for a six-layer slab. Black dotted line: symmetric slab (same data as in Fig. 1). Red solid lines: hydrogen-terminated asymmetric slab, $E_{SS}^{(6)}$ is located at the top surface and $E_{SS}^{(6)} + \Delta_H$ at the hydrogen-terminated bottom surface. (c) As panel (b), but for nine-layer slab.

combinations from the surface states of the symmetric slab are shown in the bottom panel. The top panel shows the essentially noninteracting bottom and top surface states of the hydrogen-terminated nonsymmetric slab. The high-energy

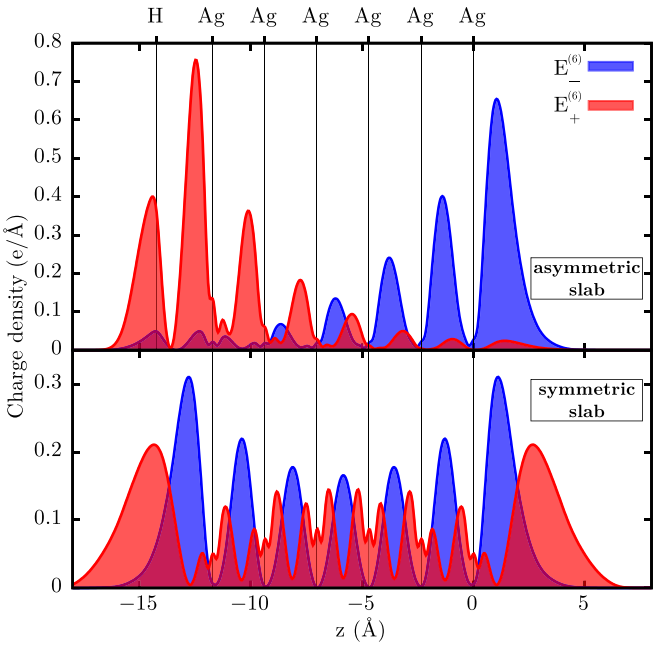

FIG. 5. Line charge densities of the Shockley states at $\vec{k}_\parallel = \Gamma$, calculated with DFT for two six-layer slabs. The charge densities are integrated over the in-plane coordinates within the unit cell. States with $E_+^{(6)}$ and $E_-^{(6)}$ are shown in red and blue, respectively. The top panel shows the results for the hydrogen-terminated asymmetric slab, where the state with $E_-^{(6)}$ is the surface state at the clean top surface and the state with $E_+^{(6)}$ is the surface state at the hydrogen-terminated bottom surface. The bottom panel displays corresponding results for the symmetric slab where the states with $E_\pm^{(6)}$ are the linear combinations of both surface states. Vertical lines indicate the substrate layers of the Ag(111) slab.

$(E_+^{(6)})$ state is located at the hydrogen-terminated surface, whereas the low-energy $(E_-^{(6)})$ state lives at the clean surface. We find that the $E_+^{(6)}$ state is strongly concentrated at the hydrogen atoms and decays much faster inside the slab than the $E_-^{(6)}$ state, the density of which looks very similar to the converged Shockley state of the 30-layer slab shown in Fig. 2. However, even for the $E_-^{(6)}$ state there still appears a small residual charge density at the hydrogen atom at the opposite surface. We note that both states exhibit only a small overlap. This overlap is additionally decreased by the faster decay of the $E_+^{(6)}$ state inside the slab. This reduces $V^{(6)}$ in Eq. (4) in comparison to its original value in Eq. (1) even further, which additionally improves the decoupling of both states.

Since the energy $E_-^{(6)}$ of the clean surface state of the hydrogen-terminated asymmetric slab is already in good agreement with E_{SS} as defined above and since its density matches the "true" Shockley state of Fig. 2, all further calculations are run with six- and nine-layer slabs with hydrogen termination on the bottom surface. In the remainder of the paper, we therefore drop the superscript M and denote the energy E_- of the surface state at the bare surface as E_{SS}. Note that the hydrogen-terminated asymmetric slab method deals only with the interaction of the opposing Shockley states but cannot eliminate their thickness (or M) dependence. However, since we are mainly interested in the subsequent effects of adding an adsorbate, we have a good basis for such investigations as long as the slab thickness M is kept constant. The adsorbate-induced changes may slightly depend on M (see Sec. III).

C. Projection technique

In the following, we present a projection technique which helps us to identify the primitive dispersion of states in large supercells, even if the latter contain additional atoms that are not contained in the primitive reference cell. The technique is particularly well suited for the analysis of the

band structure of systems with supercells that are created by adsorbates, impurities, or surface reconstructions. Besides, the projection technique can also serve as a straightforward unfolding procedure in which the primitive dispersion of an arbitrarily folded band structure is recovered. Before being able to apply the projection technique, one needs to perform self-consistent calculations of, first, the adsorbate system (or the bare surface) in the supercell (SC) and, second, the bare surface in the primitive cell (PC).

The PC is given by the atomic positions $\vec{\tau}_\nu$ and the lattice vectors $\vec{R}$, whereas the SC is denoted by the lattice vectors $\vec{Q}$ and the atomic positions $\vec{\mu}_{\tilde{\nu}}$, where

$$\vec{\mu}_{\tilde{\nu}} \equiv \vec{\mu}_{(\nu,\omega)} = \vec{\tau}_\nu + \vec{R}_\omega \quad \text{with} \quad \omega = 1\,,2\,,\ldots\,,M^{\mathrm{SC}}. \tag{5}$$

M^{SC} is the number of PCs that are contained in the SC, and $\vec{R}_\omega$ denote the lattice vectors of the PC that are needed to reach the primitive cell with label ω in the SC. For any function f the identity

$$\sum_{\vec{R}} f(\vec{R}+\vec{\tau}_\nu) = \sum_{\omega}\sum_{\vec{Q}} f(\vec{Q}+\vec{\mu}_{\nu,\omega}) \tag{6}$$

holds since SC and PC describe the same physical system. Because we are using a LCAO method, the Kohn-Sham wave functions are given by

$$\varphi_{n,\vec{k}}(\vec{r}) = \sum_{\alpha,\nu,\vec{R}} c_{\alpha,\nu,n}(\vec{k})\frac{e^{i\vec{k}(\vec{R}+\vec{\tau}_\nu)}}{\sqrt{N}}\psi_{\alpha,\nu}(\vec{r}-\vec{R}-\vec{\tau}_\nu), \tag{7}$$

where $\psi_{\alpha,\nu}$ is the localized basis function of atom ν with quantum number α, the $c_{\alpha,\nu,n}(\vec{k})$ are expansion coefficients, and N is the number of unit cells introduced in the Born–von Karman boundary conditions. The Kohn-Sham wave functions fulfill the Bloch condition for the PC. By use of Eq. (6), we can rewrite Eq. (7) to read as

$$\varphi_{n,\vec{k}}(\vec{r}) = \sum_{\alpha,\tilde{\nu},\vec{Q}} c_{\alpha,\tilde{\nu},n}(\vec{k})\frac{e^{i\vec{k}(\vec{Q}+\vec{\mu}_{\tilde{\nu}})}}{\sqrt{N}}\psi_{\alpha,\tilde{\nu}}(\vec{r}-\vec{Q}-\vec{\mu}_{\tilde{\nu}}), \tag{8}$$

where $c_{\alpha,\tilde{\nu},n}(\vec{k}) \equiv c_{\alpha,(\nu,\omega),n}(\vec{k}) = c_{\alpha,\nu,n}(\vec{k})$ and $\psi_{\alpha,\tilde{\nu}} = \psi_{\alpha,\nu}$ for each ω. Equation (8) describes the primitive wave functions with their primitive Bloch periodicity within the SC basis and lattice vectors.

Next, we calculate a scalar product of $\varphi_{n,\vec{k}}$ with an arbitrary Kohn-Sham wave function $\varphi^{\mathrm{SC}}_{m,\vec{k}}(\vec{r})$ that is *generically* defined in the SC. This wave function may correspond to a changed physical system, e.g., including adsorbates or impurities or with a surface reconstruction, thus leading to additional or missing basis functions in the basis set. This product can be written as

$$\begin{aligned}\langle\varphi_{n,\vec{k}}|\varphi^{\mathrm{SC}}_{m,\vec{k}}\rangle &= \int d^3r_1 \frac{1}{\sqrt{N}}\frac{1}{\sqrt{N^{\mathrm{SC}}}} \\ &\times\sum_{\alpha,\tilde{\nu}}\sum_{\vec{Q}''} c^*_{\alpha,\tilde{\nu},n}(\vec{k})e^{-i\vec{k}(\vec{Q}''+\vec{\mu}_{\tilde{\nu}})}\psi^*_{\alpha,\tilde{\nu}}(\vec{r}_1-\vec{Q}''-\vec{\mu}_{\tilde{\nu}}) \\ &\times\sum_{\alpha',\tilde{\nu}'}\sum_{\vec{Q}'} d_{\alpha',\tilde{\nu}',m}(\vec{k})e^{i\vec{k}(\vec{Q}'+\vec{\mu}_{\tilde{\nu}'})}\psi_{\alpha',\tilde{\nu}'}(\vec{r}_1-\vec{Q}'-\vec{\mu}_{\tilde{\nu}'}),\end{aligned} \tag{9}$$

where $d_{\alpha',\tilde{\nu}',m}(\vec{k})$ denotes the coefficients of the SC wave function. With $\vec{r} \equiv \vec{r}_1 - \vec{Q}''$, $\vec{Q} \equiv \vec{Q}' - \vec{Q}''$, and $\sum_{\vec{Q}'} 1 = N^{\mathrm{SC}}$, the scalar product of Eq. (9) can be rewritten as

$$\frac{1}{\sqrt{M^{\mathrm{SC}}}}\sum_{\alpha,\alpha',\tilde{\nu},\tilde{\nu}'} c^*_{\alpha,\tilde{\nu},n}(\vec{k})S_{\alpha\tilde{\nu},\alpha'\tilde{\nu}'}(\vec{k})d_{\alpha',\tilde{\nu}',m}(\vec{k}), \tag{10}$$

where $M^{\mathrm{SC}} = N/N^{\mathrm{SC}}$ and the overlap S is given by

$$\begin{aligned}S_{\alpha\tilde{\nu},\alpha'\tilde{\nu}'}(\vec{k}) &= \sum_{\vec{Q}} e^{i\vec{k}(\vec{Q}+\vec{\mu}_{\tilde{\nu}'}-\vec{\mu}_{\tilde{\nu}})} \\ &\times\int d^3r\,\psi^*_{\alpha,\tilde{\nu}}(\vec{r}-\vec{\mu}_{\tilde{\nu}})\psi_{\alpha',\tilde{\nu}'}(\vec{r}-\vec{Q}-\vec{\mu}_{\tilde{\nu}'}).\end{aligned} \tag{11}$$

The only requirement for being able to write $\langle\varphi_{n,\vec{k}}|\varphi^{\mathrm{SC}}_{m,\vec{k}}\rangle$ as the expression (10) is that both wave functions in the scalar product can be written in terms of the same lattice vectors $\vec{Q}$, which are fulfilled by construction. However, within the common SC the bases may differ for the two wave functions (see above), leading to a rectangular (instead of quadratic) overlap matrix S in Eq. (11).

We use the projection technique in the following way: First, we calculate the eigenstates $|\varphi_{n,\vec{k}}\rangle$ of the bare surface in the PC and expand them in the basis of the SC. Second, we calculate the eigenstates $|\varphi^{\mathrm{SC}}_{m,\vec{k}}\rangle$ of the modified system, i.e., the surface including possible reconstructions, adatoms, adsorbates, or impurities; evidently, this calculation has to proceed in the SC. Finally, we assign a weight

$$G_m(\vec{k}) \equiv \sum_n g_{m,n}(\vec{k}) \equiv \sum_n \left|\langle\varphi_{n,\vec{k}}|\varphi^{\mathrm{SC}}_{m,\vec{k}}\rangle\right|^2 \tag{12}$$

to each the of the states $|\varphi^{\mathrm{SC}}_{m,\vec{k}}\rangle$. The weights $G_m(\vec{k})$ are then used to classify individual states in a band structure. Note that the sum over n in Eq. (12) may either run over all states $|\varphi_{n,\vec{k}}\rangle$, or only over a specific subset of these states. If all states $|\varphi_{n,\vec{k}}\rangle$ are used, the projection technique simply acts as an unfolding procedure because states with primitive Bloch periodicity receive a large weight, while backfolded states get a low weight.

If the SC has no basis changes, e.g., from adsorbates or impurities, and describes the same physical system, the weights of Eq. (12) give $G_m(\vec{k}) = \{0, 1\}$ depending on the Bloch periodicity of the states. This is illustrated in Fig. 6 for the Ag(111) surface band structure. It shows the band structure of a (2×2)-SC with the color scale indicating the weights $G_m(\vec{k})$. As can be seen from the figure, the primitive dispersion

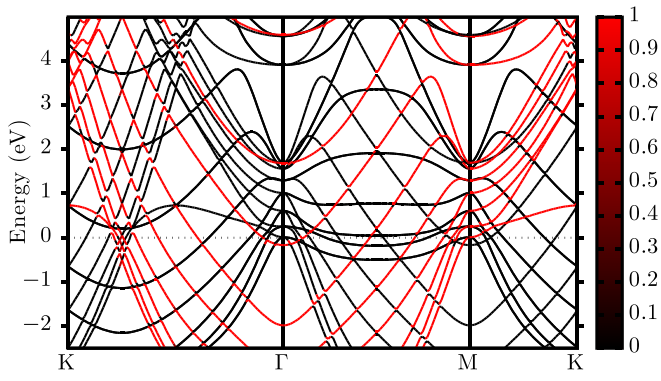

FIG. 6. Band structure for the bare Ag(111) surface within a (2×2) supercell, calculated with DFT for a hydrogen-terminated asymmetric slab. The bands are plotted in the BZ of the primitive (1×1) unit cell. The Fermi energy is set to zero. The bands are colored corresponding to their weights $G_m(\vec{k})$ as calculated in Eq. (12), where the projection was carried out over all primitive states $\varphi_{n,\vec{k}}$. Comparing the band structure in this figure to the primitive dispersion of Ag(111) in the (1×1) cell (red lines in Fig. 4), it becomes evident that the projection technique essentially unfolds the band structure of the (2×2) supercell.

is perfectly reproduced by the red bands $[G_m(\vec{k}) = 1]$. The black lines, on the other hand, stem from simple backfolding, leading to $G_m(\vec{k}) = 0$. If, on the other hand, the physical system described by the SC differs from the one described by the PC and the basis set is changed, e.g., due to the presence of adsorbates, impurities, or surface reconstructions, the weights may also take different values $[0 \leqslant G_m(\vec{k}) \leqslant 1]$.

Note that in a case where the SC has basis changes (also if it describes the same physical system), Eq. (10) is not a norm-conserving scalar product in a strict mathematical way since the Hilbert spaces of both systems differ slightly. This means that in principle $G_m(\vec{k}) > 1$ is possible. However, if the overlap elements of the matrix in (11) are not too large (e.g., achieved by placing additional basis functions not too close to those of the PC basis), the weights will show only small deviations from the strict mathematical case, as can be seen in the reference calculations of Sec. III B (see black data points in Fig. 11). This allows us to use this technique to get information about the character of the states in the SC calculation.

In this paper, we employ the projection technique as introduced above to project the states of various adsorbate-covered Ag(111) surfaces (SC) on the Shockley state of the bare Ag(111) surface (PC), thus determining the degree to which the former resemble the Shockley state of Ag(111). This allows us to discuss the origin and character of states of the adsorbate-covered surface, in particular of the interface state. It also should help us to identify and quantify splittings and interactions, especially in cases when for a particular $\vec{k}$ more than a single state with Shockley character is present.

III. RESULTS

A. Carbon monoxide test system

We choose a (1×1) monolayer of carbon monoxide (CO) adsorbed on the Ag(111) surface to test whether the hydrogen-terminated asymmetric slabs introduced in Sec. II B are suitable for investigating adsorption-induced changes of the surface band structure. Because this system shows the same (1×1) periodicity as the clean Ag(111) surface, we can indeed perform a 30-layer symmetric slab calculation for benchmarking our asymmetrically passivated thin-slab calculations. The structure of the system is shown in Fig. 7(a). Note that we artificially place the CO molecules at a Ag-C distance of 3 Å because this corresponds to the typical Ag-C distance for the NTCDA/Ag(111) system which we analyze later on in Sec. III B. The bond length between the carbon and oxygen atoms is set to 1.2 Å. The calculations of this system are carried out using the same basis functions at the positions of Ag atoms as we used for the bare Ag(111) surface in Sec. II B, but including additional localized wave functions placed at the positions of the C and O atoms of the CO molecules.

TABLE I. Parameters of the Shockley state of the Ag(111) surface and the interface state of the CO/Ag(111) system, derived from the fits in Figs. 7(c) and 8(a) and 8(b). Layers: number of Ag layers in the slab of the DFT calculation. The calculations with 6 and 9 layers employ a hydrogen-terminated asymmetric slab, the calculation with 30 layers a symmetric slab. The effective masses are given in units of the electron mass m_e and the energies are given in meV. The reference values for the Shockley state were calculated including the basis set of the CO molecule.

Layers	E_{SS} [50]	m^*_{SS}	E_{IS}	m^*_{IS}	ΔE	Δm
6	−198	0.42	468	0.55	666	0.13
9	−84	0.37	576	0.48	660	0.11
30	−39	0.34	598	0.45	637	0.11

The results for the reference calculation with the converged symmetric 30-layer slab without hydrogen passivation are shown in Fig. 7(b). There are two states with a parabolic dispersion around Γ in the gap of surface-projected bulk band structure. The low-energy state is the Shockley state ($E_{SS} = -39$ meV) at the bare bottom surface of the 30-layer slab (cf. Fig. 1), while the high-energy state ($E_{IS} = 598$ meV) is the interface state resulting from the adsorption of CO at the top surface. Two additional CO-induced dispersing bands ($E \sim 4$ eV) occur in the band structure. These states are also (partially) located in the gaps of surface-projected bulk band structure, but interact with neither the Shockley state nor the interface state.

We use parabolic fit functions to determine the effective masses of the interface state and the Shockley state as shown in Fig. 7(c). The fits were performed in the interval $\Gamma \pm 0.2\,\frac{\pi}{a}$, where a is the lattice constant of Ag. The onset energies and effective masses obtained by the fit are listed in Table I. To avoid systematic errors due to different basis sets, the reference values for E_{SS} in Table I are calculated including the localized basis functions of the CO molecule. This leads to small changes of E_{SS} compared to the results in Sec. II B. In the 30-layer symmetric slab calculation for CO/Ag(111) we find an interface state that is located $\Delta E \equiv E_{IS} - E_{SS} = 637$ meV above the Shockley state of the bare Ag(111) surface. The effective mass of the interface state ($m^*_{IS} = 0.45\,m_e$) is larger than one of the corresponding Shockley state

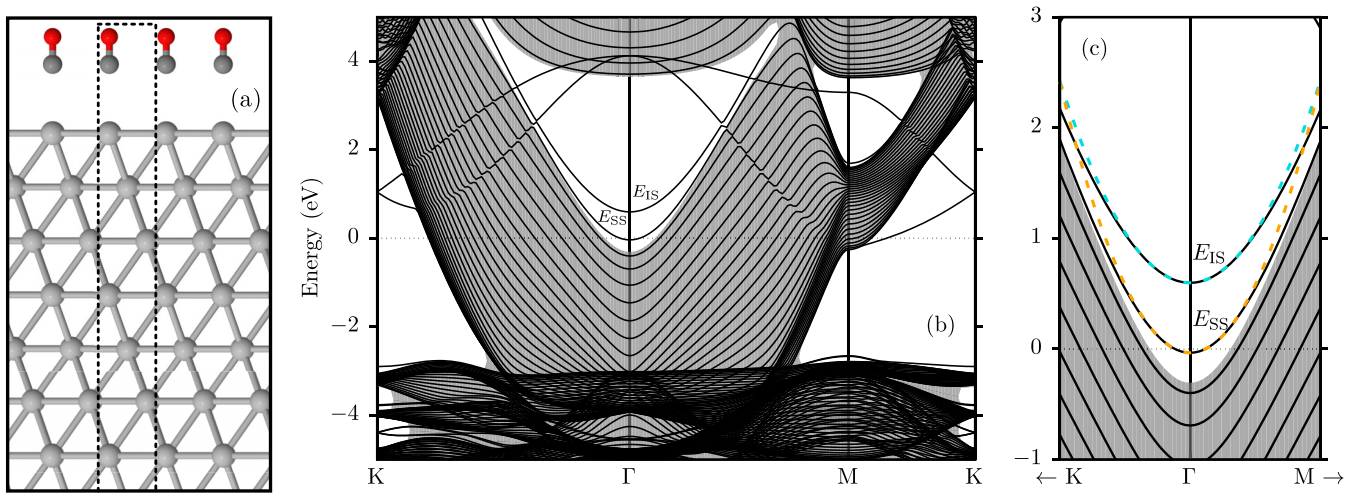

FIG. 7. The CO/Ag(111) test system. (a) Side view of the unit cell. The carbon atoms (dark gray) are located 3 Å above the silver surface (light gray). The bond length to the oxygen atom (red) is set to 1.2 Å. The unit cell is indicated by the black dashed line. (b) Band structure for the CO/Ag(111) test system, calculated with a 30-layer symmetric slab. The Fermi energy is set to zero. The gray area shows the surface-projected band structure of the bulk crystal. (c) Zoom into the region of the Ag(111) Shockley state (E_{SS}), located at the bottom surface of the slab, and the CO/Ag(111) interface state (E_{IS}) at the top surface. Orange dashed line: surface state dispersion fitted with a quadratic function. Blue dashed line: interface state dispersion fitted with a quadratic function. The fit parameters are listed in Table I.

($m^*_{\mathrm{SS}} = 0.34\,m_e$). As will be discussed below, the renormalization of the effective mass is a generic effect of the adsorbate and in the case of NTCDA even leads to a pronounced anisotropy of the interface state dispersion.

We now compare the 30-layer symmetric slab calculation to corresponding ones on hydrogen-terminated asymmetric six- and nine-layer slabs. The results of the latter calculations are shown in Fig. 8, in red for the CO/Ag(111) top surface and in black for bare Ag(111) top surface, which however include the CO basis set, unlike the corresponding calculations in Figs. 4(b) and 4(c). The first noticeable feature in Fig. 8 is that the surface state of the hydrogen-passivated bottom surface (E_+, see Sec. II B) is nearly unaffected by the adsorption of CO. In the six-layer calculation it shifts by about 50 meV to higher energy, for the nine-layer calculation this shift amounts to only 10 meV. Second, also in the hydrogen-terminated asymmetric slab calculations the CO/Ag(111) interface state appears at higher energies if compared to the Shockley state of the bare Ag(111) surface. For the six-layer asymmetric slab, the corresponding energy difference is $\Delta E = 666$ meV, while for the nine-layer asymmetric slab it amounts to $\Delta E = 660$ meV (Table I). Comparing these energy differences to the one for the 30-layer symmetric slab ($\Delta E = 637$ meV), we find that all three are within 5% of each other. Finally, we compare the effective masses resulting from the three calculations. Although the absolute value of m^*_{IS} obtained with the 30-layer symmetric slab is not reproduced with thinner asymmetric slabs, its *increase* $\Delta m \equiv m^*_{\mathrm{IS}} - m^*_{\mathrm{SS}}$ is confirmed by the latter (see Table I).

We thus conclude that thin asymmetric slabs that are hydrogen terminated at the bottom surface are indeed a viable approach to investigate adsorption-induced changes of the Shockley state at the top surface. In our test system, the energy difference between the surface state and the interface state after adsorption is described with an accuracy of better than 5% even with the minimalistic six-layer slab. Although the exact values of the effective masses still depend on the number of layers in the slab, their increase caused by the adsorbate can be reproduced very well, by the nine-layer slab slightly better than by the six-layer slab. Nevertheless, even the 6-layer slab reproduces all the systematic trends that are observed for 9-layer slab (and the 30-layer symmetric slab). Having

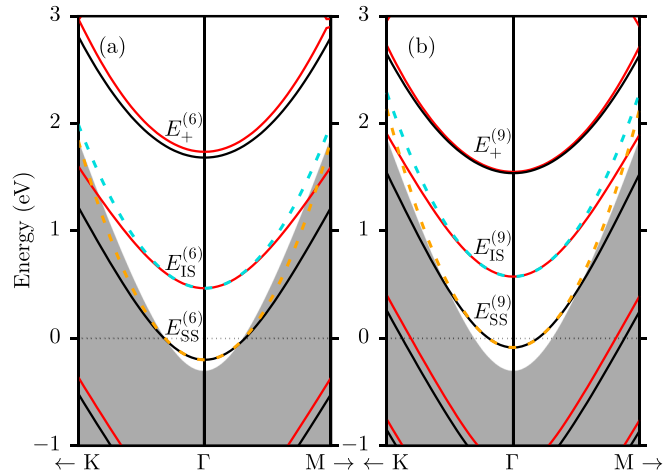

FIG. 8. Band structure around the Γ point for the CO/Ag(111) test system (red lines), calculated with DFT using (a) a six-layer hydrogen-terminated asymmetric slab and (b) a nine-layer hydrogen-terminated asymmetric slab. The gray area shows the surface-projected band structure of the bulk crystal. For reference, the band structures of the Ag(111) surface without the adsorbate [analogous to Figs. 4(b) and 4(c) but including the basis orbitals of the CO molecule] are plotted in black. All energies are defined relative to the corresponding Fermi energy. Orange dashed line: surface state dispersion fitted with a quadratic function. Blue dashed line: interface state dispersion fitted with a quadratic function. The fit parameters are listed in Table I.

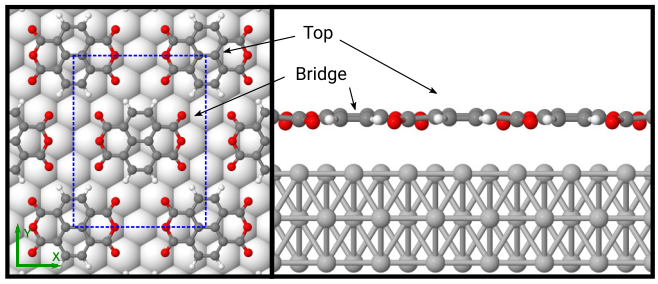

FIG. 9. Unit cell of the NTCDA monolayer in the experimentally observed relaxed phase [24]. The dashed blue line marks the unit cell. Left: top view, showing one molecule each in top and bridge positions. The green arrows mark the x and y directions. Right: side view, showing the bending of the layer above the surface.

thus validated the hydrogen passivation technique as a means for efficient surface and interface state calculations, we are now finally equipped for the analysis of the NTCDA/Ag(111) interface electronic structure.

B. Interface state of NTCDA/Ag(111)

Here we concentrate on the analysis of structures that stem from the commensurate monolayer of NTCDA on Ag(111) characterized by the superstructure matrix $\begin{pmatrix} 4 & 0 \\ 3 & 6 \end{pmatrix}$ [24]. The rectangular unit cell of this so-called relaxed phase monolayer contains two molecules per unit cell, all of which are aligned with their long axis along the $[1\bar{1}0]$ direction of the Ag(111) surface. While the precise adsorption configuration of both molecules has not yet been determined experimentally, we follow Ref. [24] and assume that one of them adsorbs in an on-top position, while the other sits in a bridge site (Fig. 9). This assumption agrees with published theoretical results [19]. At these lateral positions, we carry out a geometry optimization as described in Sec. II A. Note that we only relax the atoms in the molecules, but not in the silver surface.

TABLE II. Calculated vertical distances in Å of individual chemical species within the NTCDA molecules adsorbed on Ag(111). *Isolated* refers to an isolated molecule, adsorbed in a bridge position and calculated in a (8×8) unit cell. *Top* and *bridge* refer to molecules in on-top and bridge positions within the relaxed monolayer phase, respectively. $\overline{d}$ is averaged over all atoms within the molecule, $\overline{d}_C$ is averaged over all carbon atoms within the molecule. The averaged distances of the oxygen atoms are denoted as d_O^{carb} for the carbonyl oxygens and d_O^{anh} for the anhydride oxygens. d_H is the averaged distance of the hydrogen atoms. The table also contains the vertical extent Δz that quantifies the overall buckling amplitude of the molecule. The last line contains the experimental values measured at room temperature [51].

	$\overline{d}$	$\overline{d}_C$	d_O^{carb}	d_O^{anh}	d_H	Δz
Isolated	2.86	2.94	2.66	2.88	2.82	0.38
Top	2.89	2.96	2.70	2.91	2.88	0.35
Bridge	2.86	2.94	2.65	2.90	2.84	0.39
Expt. [51]		2.997	2.747	3.004		

The resulting vertical distances to the surface, averaged over all atoms of a given species, are shown in Table II. The comparison of our data regarding the average carbon-surface distance $d_C = 2.95$ Å with experiments (3.00 Å) shows a reasonable agreement. However, we note that the experimental value was obtained at room temperature [51], whereas we calculate the ground-state distance at $T = 0$ K. This indicates that our calculations may overestimate d_C by as much as 0.2 Å [52].

Having optimized the molecular geometry, we perform a DFT band structure calculation with hydrogen-terminated asymmetric six- and nine-layer silver slabs, using a (16×12) $\vec{k}_\parallel$ grid. The band structure of the NTCDA monolayer on the six-layer slab, displayed in the primitive (1×1) BZ of bare Ag(111), is shown in Fig. 10(a). The corresponding path through reciprocal space is shown in Fig. 10(b). To

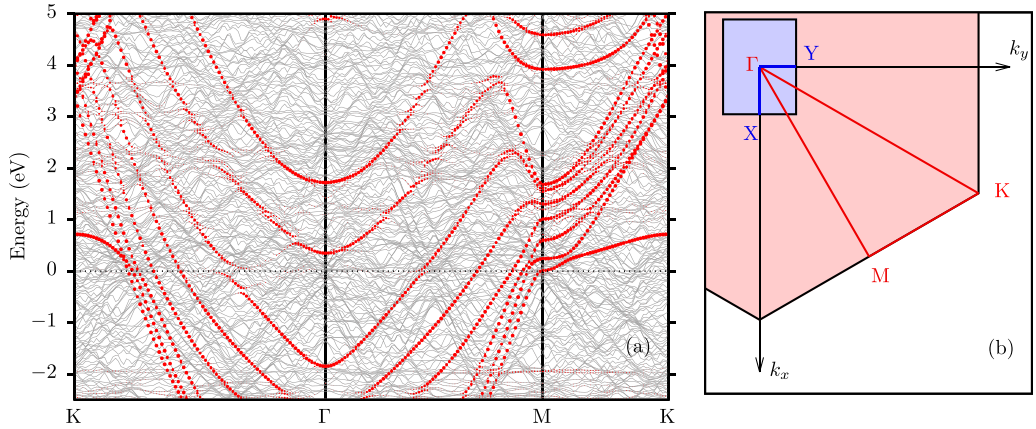

FIG. 10. The NTCDA/Ag(111) system. (a) Band structure of the relaxed phase of NTCDA/Ag(111), calculated with DFT for a hydrogen-terminated asymmetric six-layer slab, displayed in the primitive (1×1) BZ of the bare Ag(111) surface. The Fermi energy is set to zero. The red dots show the projection onto the states of the Ag(111) surface. The area of the dots is proportional to the weights $G_m(\vec{k})$ from Eq. (12), where the projection was carried out over all primitive states. (b) The surface BZ of the NTCDA monolayer (blue) embedded in the surface BZ of the Ag(111) surface (red). The corresponding band structure paths are plotted as red and blue lines. The k_x and k_y directions match the x and y directions of Fig. 9.

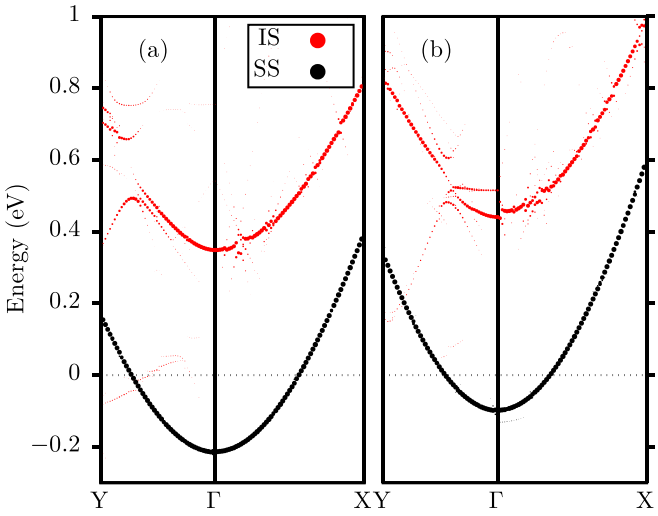

FIG. 11. DFT-calculated interface state of the relaxed phase of NTCDA/Ag(111) (red) and Shockley state of bare Ag(111) (black), both plotted as projection weights $G_m(\vec{k})$ as defined in Eq. (12), in the BZ of the rectangular NTCDA supercell [Fig. 10(b)]. The area of the dots is proportional to the weights $G_m(\vec{k})$. The sum in Eq. (12) was carried out only over the Shockley state of bare Ag(111), which corresponds to a projection onto this state. (a) Results for hydrogen-terminated asymmetric six-layer slab. (b) Results for hydrogen-terminated asymmetric nine-layer slab. For each number of layers, calculations for the surface (black) and interface (red) states were carried out in the NTCDA/Ag(111) supercell using exactly the same basis set and calculation parameters. All Fermi energies are set to zero. For clarity, the underlying bands are not plotted.

analyze this complex band structure, the projection technique introduced in Sec. II C is employed to map the states of the NTCDA/Ag(111) system (SC) onto those of the original (1 × 1) Ag(111) system (PC). The solid red dots in Fig. 10 mark states for which $G_m(\vec{k}) \approx 1$, with the sum in Eq. (12) carried out over all states of the (1 × 1) Ag(111) system. As discussed above, this can be thought of as an unfolding procedure in which states with a primitive Bloch periodicity receive large weights, provided that these states have considerable overlap with at least one of states in the original (1 × 1) Ag(111) system. Figure 10(a) thus not only reveals that all states of the bare (1 × 1) Ag(111) in Fig. 4(a) "show up" also in Fig. 10(a) because they have counterparts among the states of the NTCDA/Ag(111) system (as expected for unfolding), but also that most states of the bare (1 × 1) Ag(111) persist with almost unchanged energies in the NTCDA/Ag(111) system. There is, however, one exception, and that is the Shockley state of the bare (1 × 1) Ag(111) surface: Its counterpart with $G_m(\vec{k}) \approx 1$ in Fig. 10(a) appears at substantially larger energy. By analogy with CO/Ag(111) as discussed in Sec. III A (Fig. 7), we can identify this counterpart as the interface state of NTCDA/Ag(111).

To analyze the relation between the NTCDA/Ag(111) interface state and the Ag(111) Shockley surface state further, we project all states of NTCDA/Ag(111) onto the (1 × 1) Ag(111) Shockley state only [i.e., the sum in Eq. (12) now contains only the Shockley state]. The result is the band shown in Fig. 11 in red, for the six-layer hydrogen-terminated asymmetric slab in Fig. 11(a) and the corresponding nine-layer slab in Fig. 11(b). Only the weights themselves, with no underlying bands, are shown. Figure 11 shows that *only* one state of NTCDA/Ag(111) has a sizable overlap with the (1 × 1) Ag(111) Shockley state, and this clearly must be the interface state. In order to avoid systematic errors due to different basis sets, we compare the interface state band in Fig. 11 with the Shockley state that is obtained if we recalculate the bare Ag(111) surface with the same basis set and precisely the same computational parameters as are used for NTCDA/Ag(111). If the resulting band structure is projected on the Shockley state, we observe the weights shown as black dots in Fig. 11. Not surprisingly, this self-projection filters out only the Shockley state band with weight $G_m(\vec{k}) = 1$.

TABLE III. Calculated energy and effective mass of the Shockley state of the bare silver surface and interface state for the NTCDA monolayer on a six- and nine-layer slab. The shifts are compared to experimental two-photon photoemission (2PPE) data [19], whereas the effective masses are compared to our experimental dispersion measured from FT-STS. All values are given in meV or m_e, respectively. The reference values for the Shockley state were calculated including the basis set of the NTCDA monolayer.

Layers	E_{SS} [50]	m^*_{SS}	E_{IS}	$m^*_{IS,x}$	$m^*_{IS,y}$	ΔE
6	−213	0.42	349	0.54	0.39	562
9	−98	0.37	455	0.49	0.40	553
2PPE [19]	−60		520			580
STS	−67 [53]	0.42 [53]	570	0.55	0.35	637

We now proceed to compare the red and black bands in Fig. 11. The corresponding onset energies at $\vec{k}_\parallel = \Gamma$ are listed in Table III. Similarly to CO, the adsorption of NTCDA leads to the formation of an interface state that has a higher energy than the Shockley surface state. For the six-layer slab $\Delta E^{(6)} = 562$ meV, while $\Delta E^{(9)} = 553$ meV for the nine-layer slab. Both values are close to $\Delta E^{2ppe} = 580$ meV as measured by two-photon photoemission at 90 K [19]. They also agree with recent theoretical results [18,19]. As will be shown below, the ΔE^{STS} measured at low temperatures with STS is higher, most probably due to the expected temperature-dependent decrease of the bonding distance [52]. In spite of this discrepancy, we conclude that our six- and nine-layer hydrogen-terminated asymmetric slab calculations perform reasonably well in reproducing the energy spectrum of the NTCDA/Ag(111) interface state.

Comparing the surface and interface states in Fig. 11 more carefully, a subtle difference comes into focus: the interface state (red) appears to have different curvatures along the k_x and k_y directions. In contrast, such an anisotropy is not observed for the surface state (black). Since both bands in Fig. 11 have been calculated in precisely the same way, it is unlikely that the anisotropy of the interface state is an artifact of either the hydrogen termination or the projection technique. The visually inferred anisotropy of the interface state is confirmed by fitting its dispersion in the interval $|\vec{k}| = 0.04\ \frac{\pi}{\text{Å}}$ with parabolas. For the six-layer slab, we find effective masses of $m^*_{IS,x} = 0.54 m_e$ along ΓX and of $m^*_{IS,y} = 0.39 m_e$ along ΓY [cf. the NTCDA/Ag(111) BZ in Fig. 12]. For

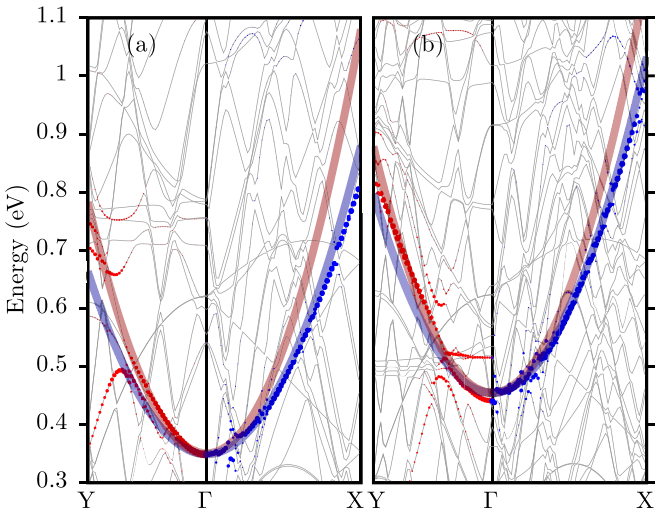

FIG. 12. DFT-calculated interface state of the relaxed phase of NTCDA/Ag(111) as in Fig. 11, with the exception that the underlying bands are also shown (thin gray lines). (a) Results for hydrogen-terminated asymmetric six-layer slab. (b) Results for hydrogen-terminated asymmetric nine-layer slab. As in Fig. 11, the area of the dots is proportional to the projection weights $G_m(\vec{k})$, with data points along the ΓX direction shown in blue and data points along the ΓX direction in red. The red and blue lines are quadratic fits to the interface state dispersion as revealed by the projection weights, carried out separately for the two k-space directions. For ease of comparing the curvatures, the blue (red) parabolas have been mirrored to the left (right). The Fermi energy is set to zero.

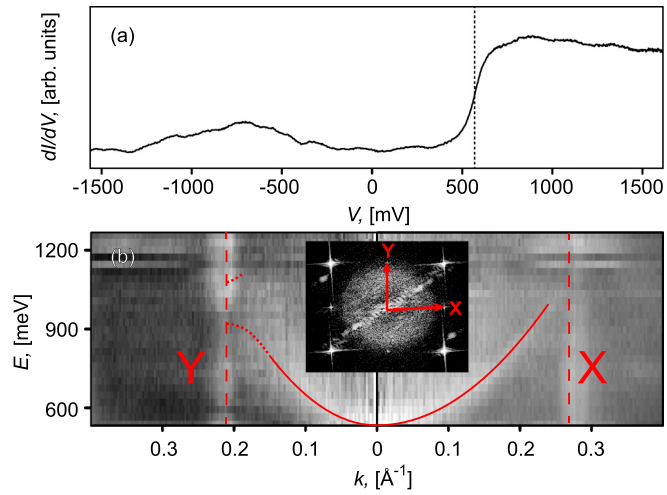

FIG. 13. STS of the relaxed phase of NTCDA/Ag(111). (a) dI/dV spectrum measured above an NTCDA island far away from its boundaries and any defects. The peak below −500 meV indicates the position of the NTCDA LUMO [filled upon adsorption on Ag(111)], while the steplike feature at 570 meV marks the onset of the interface state band. (b) Grayscale image of the interface state band, obtained from cuts through 2D Fourier transforms of an energy series of large-scale dI/dV images of an NTCDA/Ag(111) island which contains many scattering defects. Details about the data acquisition and analysis in FT-STS can be found in Ref. [23]. The left (right) part of the panel shows the dispersion along the ΓY (ΓX) direction. The BZ boundaries corresponding to the NTCDA/Ag(111) superstructure are indicated by red vertical dashed lines. Two half-parabolas (red) with $m_x^* = 0.55\,m_e$ and $m_y^* = 0.35\,m_e$ are placed over the data. The gap that is identified by FD-STS (see Fig. 14) is designated with the dotted red line close to the Y point. The inset shows one ($V = 860$ meV) from the series of FFT images used to compile the grayscale image of the interface state band. Red arrows indicate the BZ boundaries [23]. The elliptic shape of the central FFT disk is a direct consequence of the anisotropy of the interface state dispersion.

the nine-layer slab, the anisotropy is somewhat smaller, but still clearly recognizable and of the same sense $m^*_{\mathrm{IS},x} > m^*_{\mathrm{IS},y}$ (Table III). Figure 12 indeed demonstrates that for both slabs the anisotropy is clearly above the uncertainty of the calculated band structure. However, there is a discrepancy between the six- and nine-layer slab calculations: For the six-layer slab we find $m^*_{\mathrm{SS}} > m^*_{\mathrm{IS},y}$, while the nine-layer slab has $m^*_{\mathrm{SS}} < m^*_{\mathrm{IS},y}$. For both slabs, $m^*_{\mathrm{SS}} < m^*_{\mathrm{IS},x}$ holds.

The anisotropy of the NTCDA/Ag(111) interface state dispersion is intriguing because it follows the rectangular symmetry of the NTCDA supercell rather than the threefold symmetry of the Ag(111) surface. The anisotropy therefore clearly points toward a quantum-mechanical interaction between the metallic Shockley state and the molecular adsorbate layer. Such interaction can cause quantum-mechanical scattering, as well as hybridization between the two states. In the next section, we will see that this anisotropy is also observed in the experiment.

C. Experimentally measured dispersion of NTCDA/Ag(111)

In order to verify the theoretically predicted anisotropy of the NTCDA/Ag(111) interface state we have analyzed it with scanning tunneling spectroscopy (STS). The experimental dI/dV spectrum shown in Fig. 13(a), measured above the center of a large defect-free NTCDA island, reveals that the onset energy of the NTCDA/Ag(111) interface state, defined by the steplike spectral feature, is located 570 meV above the Fermi level. This is $\Delta E^{\mathrm{STS}} = 637$ meV higher than the experimentally measured energy of the Ag(111) Shockley state. Here, as well as in the case of PTCDA/Ag(111) [11], STS yields systematically higher onset energies of the interface band compared to the two-photon photoemission (2PPE) data [19,54]. Since our STS spectra are measured at a lower temperature than the 2PPE spectra (4 K vs 90 K), we attribute the observed discrepancy to the temperature dependence of the molecule-metal bonding distance [12,22,52].

Spectroscopically imaging the NTCDA/Ag(111) interface at a set of bias voltages ranging from 500 to 1300 meV and using the thus obtained dI/dV images for an analysis by Fourier transform scanning tunneling spectroscopy (FT-STS) [23,55], we map out the dispersion of the NTCDA/Ag(111) interface band in the vicinity of the Γ point. The result is shown in Fig. 13(b). The visual inspection of the experimental data reveals that the dispersion of the NTCDA/Ag(111) interface state exhibits a notable anisotropy. We find effective masses of $m^*_{\mathrm{IS},x} \simeq 0.55 m_e$ and $m^*_{\mathrm{IS},y} \simeq 0.35 m_e$, as overlaying the experimental image in Fig. 13(b) with corresponding parabolas shows. The experimentally found anisotropy is thus in good quantitative agreement with the theoretically predicted one (cf. Table III).

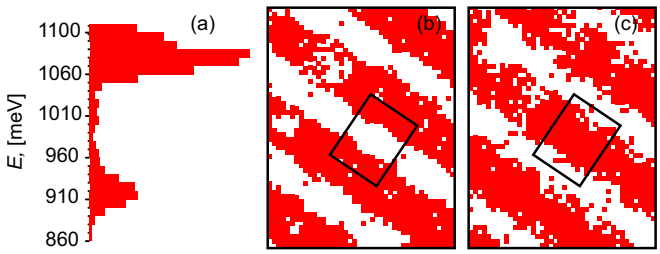

FIG. 14. FD-STS of the relaxed phase of NTCDA/Ag(111). (a) Section of the energy distribution histogram (EDH) extracted by FD-STS (for details see Ref. [23]). The two peaks of the histogram define the lower and upper band edges around the energy gap of the interface state at the Y point. (b) Feature distribution map (FDM) extracted from the lower peak of the EDH (see Ref. [23]). (c) FDM extracted from the upper peak of the EDH. Each of the FDM in panels (b) and (c) covers an area of 47×61 Å^2, revealing standing wave patterns caused by Y-point Bragg scattering of the interface state. Coincident unit cells of the relaxed NTCDA/Ag(111) monolayer in both FDM are indicated by black rectangles.

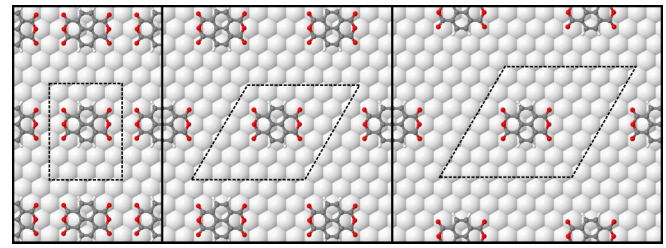

FIG. 15. Real-space unit cells of dilute NTCDA layers on Ag(111). The frame on the left shows the original relaxed monolayer, but with the molecules in on-top positions removed, yielding a coverage of $c = \frac{1}{2}$. The frame in the middle shows one molecule in a (6×6) supercell, giving an adsorption coverage of $c = \frac{1}{3}$. The frame on the right corresponds to a molecule in a (7×7) supercell, producing a coverage $c = \frac{12}{49} \approx \frac{1}{4}$. The respective unit cells are marked by black dashed lines.

In Sec. III B above we have pointed out that the observed anisotropy indicates quantum-mechanical interaction between the metal Shockley state and the molecular adsorbate. In fact, our experiments provide an additional piece of evidence for the existence of such an interaction: Namely, we resolve a 180 meV energy gap at the Y point, which is located on the BZ boundary of the NTCDA superstructure. Such a gap indicates the scattering of the interface state electrons in a lateral potential with the periodicity of the NTCDA/Ag(111) supercell. The gap is resolved with the help of feature detection STS (FD-STS). This is an approach to STS imaging which we have introduced recently [23]. FD-STS overcomes certain limitations of FT-STS which, in the vicinity of the BZ boundaries, is hampered by any signal that originates from the periodic topography of the corresponding unit cell [cf. inset of Fig. 13(b)]. As detailed in Ref. [23], the application of FD-STS in the present case enables us to decouple the signal that arises from the scattering of the interface state by the molecular superstructure from the signal that is generated by topographic structure of the molecular layer.

Briefly, FD-STS proceeds as follows: First, dI/dV spectra are recorded on a dense grid (e.g., 2 pixels/Å) of points above the NTCDA/Ag(111) monolayer. Then, each of the collected dI/dV spectra is run through a feature detection algorithm which determines the energies and the intensities of all peaks in the spectrum. Next, the complete detection statistics is compiled into an energy distribution histogram (EDH) in which each peak testifies to a large number of dI/dV spectra exhibiting a peak of sufficient intensity at precisely this energy. A section of this histogram for NTCDA/Ag(111) is shown in Fig. 14(a). Finally, we mark all pixels of the scanned grid which contribute to the detection statistics of a specific histogram peak. This generates a feature distribution map (FDM). The FDM of the two peaks in the EDH of Fig. 14(a) is displayed in Figs. 14(b) and 14(c). They reveal two standing wave patterns with the periodicity of the NTCDA superstructure, but shifted by half a lattice constant against each other.

A pair of standing waves such as the one observed in Figs. 14(b) and 14(c) is the hallmark of Bragg scattering of nearly free electrons in a weak periodic potential. The energies of these standing waves correspond to the lower and upper band edges around the gap that forms at the BZ boundary due to Bragg scattering. The distance between the EDH peaks in Fig. 14(a) thus reveals the size of this gap, in the present case 180 meV. Although a comparable energy gap is expected at the X boundary of the BZ, we have not been able to confirm or rule out its existence due to difficulties in measuring dI/dV of NTCDA/Ag(111) at the elevated bias voltages.

The presence of the band gap in the interface state dispersion at the Y point is a significant deviation from the DFT data discussed in Sec. III B. Although our projection technique should in principle be able to reveal such a gap, there is no sign of it in our present calculation. We point out, however, that interface state properties strongly depend on the adsorption geometry, and we have mentioned above that our calculations may overestimate the adsorption height by as much as 0.2 Å [52] because the accurate description of metal-organic interface geometries is still a challenging task for DFT. If also the opening of gaps in the calculation sensitively depends on the adsorption height, then the absence of gaps in the calculation may be the result of an inaccurately described interface structure. Apparently, in the long-wavelength limit, the correct description of the interface state is less dependent on the exact geometry of the molecular layer.

D. Coverage dependence of the interface state

Finally, we analyze the dependence of the NTCDA/Ag(111) interface state on the molecular coverage. The computational advantage of the reduced silver slab thickness allows us to increase the lateral size of the NTCDA supercells substantially. Specifically, we employ the six-layer hydrogen-terminated asymmetric slab to investigate diluted NTCDA monolayer structures, the unit cells of which are shown in Fig. 15. Although these structures are not naturally occurring, they could be produced by the controlled removal of molecules with the tip of a scanning probe microscope [56,57]. The theoretical data reported in this section

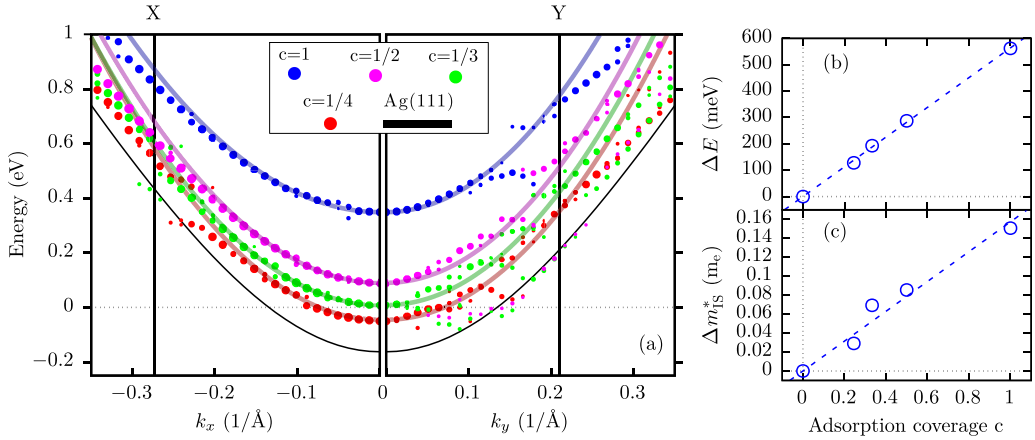

FIG. 16. NTCDA/Ag(111) interface state for different molecular coverages. (a) Dispersion as calculated with DFT for hydrogen-terminated asymmetric six-layer slabs. Colors indicate the coverage: $c = 1$ (blue), $c = \frac{1}{2}$ (magenta), $c = \frac{1}{3}$ (green), $c \simeq \frac{1}{4}$ (red). The area of the dots is proportional to the projection weights $G_m(\vec{k})$ [Eq. (12)]. The sum in Eq. (12) was carried out only over the Shockley state, which corresponds to a projection onto this state. For clarity, the underlying bands are not displayed. As a reference, the Shockley state for the bare Ag(111) surface from Fig. 12 is displayed as a thin black line (see Sec. II B). The boundaries of the BZ of the relaxed phase ($c = 1$) are denoted by X and Y. The thick solid lines are quadratic fits that were made separately for each direction to determine the corresponding effective masses. (b) Energy shift of the interface state with respect to the former Shockley state as a function of adsorption coverage. (c) Anisotropy $\Delta m^*_{IS} \equiv m^*_{IS,x} - m^*_{IS,y}$ of the interface state for different adsorption coverages. Dashed lines in (b) and (c) are guides to the eye.

thus demonstrate that the controlled patterning of an organic monolayer can be utilized for tuning the properties of the interface state.

The first artificial structure that we analyze is a half-monolayer of NTCDA with the coverage $c = \frac{1}{2}$; it is obtained by removing from the relaxed phase all molecules adsorbed in on-top sites, leaving those in bridge sites behind. Furthermore, we investigate two even more dilute structures with coverages $c = \frac{1}{3}$ and $c = \frac{12}{49} \approx \frac{1}{4}$. They are obtained by placing NTCDA molecules in bridge positions in (6×6) and (7×7) unit cells, respectively. Since the NTCDA molecules in these large superstructures do not interact with each other [58], we carry out the structural optimization in a (8×8) superstructure and then adopt the resultant molecular geometry in the (6×6) and (7×7) unit cells. As Table II demonstrates, this yields only small changes in the molecular geometry compared to the relaxed monolayer.

Having calculated the $c = \frac{1}{2}$, $\frac{1}{3}$, and $\frac{1}{4}$ layers using six-layer hydrogen-terminated asymmetric silver slabs, we apply our projection technique to determine the dispersion and the onset energy of the corresponding interface states. We employ a (8×8) $\vec{k}_\parallel$ grid for $c = \frac{1}{3}$ and $\frac{1}{4}$. All other parameters of the calculation remain identical to the monolayer ($c = 1$) calculation described above. To avoid basis set errors, for each coverage we carry out a reference calculation of the bare Ag(111) surface that includes the corresponding localized basis functions of the adsorbate molecules.

The dispersion along the ΓX and ΓY directions of the relaxed-phase NTCDA monolayer BZ [see Fig. 10(b)] is displayed in Fig. 16(a) for the different coverages. The parabolic fits have been performed in the interval $\Gamma \pm 0.04 \frac{\pi}{\text{Å}}$ to determine the onset energies and effective masses plotted in Fig. 16(b) and listed in Table IV. We find that the energetic difference $\Delta E \equiv E_{IS} - E_{SS}$ increases linearly with adsorption coverage. This result is in agreement with recent experimental and theoretical findings regarding the coverage dependence of the interface states. For example, in case of PTCDA/Ag(111), the disordered low-temperature phase [59] as well as the square phase (both with $c < 1$) have lower onset energies of the interface state (and hence lower ΔE) than the $c = 1$ herringbone structure [11,12]. Similarly, for the NTCDA/Ag(111) system, the coverage dependence of the interface state has been discussed in terms of two different commensurate structures, with the result that at same bonding distance a larger onset energy is found for the compressed, and a smaller onset for the relaxed phase [19].

Figure 16(c) in which $\Delta m^*_{IS} \equiv m^*_{IS,x} - m^*_{IS,y}$ is plotted versus NTCDA coverage shows that the anisotropy of the effective masses also increases linearly with increasing NTCDA coverage. For the lowest coverage ($c = \frac{1}{4}$), there is hardly an anisotropy, and the observed effective masses $m^*_{IS,x}$ and $m^*_{IS,y}$ are very close to the effective mass m^*_{SS} of the Ag(111) Shockley surface state. Table IV reveals that the increase of $m^*_{IS,x}$ is more pronounced than the minute decrease of $m^*_{IS,y}$. These findings thus clearly reveal the influence that the lateral structure of the molecular film has on the properties of the

TABLE IV. Parameters of the interface state of NTCDA/Ag(111) for various adsorption coverages, derived from the fits in Fig. 16(a). The effective masses are given in units of the electron mass m_e and the energies are given in meV. The energy shift was calculated with respect to the Shockley state energy obtained in a reference calculation using the same basis set.

Adsorption coverage	0	1/4	1/3	1/2	1
ΔE (meV)	0	128	193	287	562
$m^*_{IS,x}$ (m_e)	0.42	0.45	0.47	0.48	0.54
$m^*_{IS,y}$ (m_e)	0.42	0.42	0.41	0.40	0.39

interface state. Nanoscale patterning of an ordered molecular layer could thus be used to tailor its electronic, transport, and optical interface properties, in a similar way as has been achieved through the artificial placement of molecules such as CO on, e.g., Cu(111) surfaces [60,61].

IV. SUMMARY

Using *ab initio* DFT we have predicted the anisotropy of dispersion of the interface state of NTCDA/Ag(111). The DFT study was facilitated by the implementation of two technical procedures: First, we have shown that the coupling of the Shockley states of the two surfaces of the Ag(111) slab can be suppressed by hydrogen passivation of one of the slab surfaces. As a consequence of such symmetry breaking, the discussion of adsorption-induced interactions of the Shockley state becomes meaningful, even for slabs of only six atomic layers of silver. Because calculations with thinner slabs are computationally much more efficient we have been able to compute the electronic structure of the NTCDA/Ag(111) interfaces for different coverages with very large supercells. Second, we have developed a projection technique which maps the states of the surface supercell on the original dispersion of the Shockley state as observed in the primitive unit cell of Ag(111) and thus is used to identify the parameters of the dispersion of the interface state.

In agreement with experimental data in case of full NTCDA monolayer adsorption, the interface state from our calculations occurs at higher energy as the Shockley state of the bare Ag(111) surface with an energy difference of $\Delta E = 560$ meV. Moreover, we predicted a pronounced anisotropy of the dispersion along the X and Y directions of the molecular layer BZ characterized by the corresponding effective mass values of $m^*_{\mathrm{IS},x} = 0.54m_e$ and $m^*_{\mathrm{IS},y} = 0.39m_e$. This anisotropy of the interface state dispersion has been fully confirmed by our STS experiments. The STS data have also revealed the 180-meV energy gap at the Y boundary of the molecular layer BZ. Interestingly, the dispersion obtained form the DFT data had no signs of the energy gaps of comparable size. However, as the opening of gaps might be strongly depending on the correct description of the vertical binding and internal structural properties of the molecular layer, this points toward further structural investigations beyond our current DFT approach. We find that the anisotropy of the effective mass $\Delta m^*_{\mathrm{IS}} := m^*_{\mathrm{IS},x} - m^*_{\mathrm{IS},y}$ as well as the energetic difference ΔE with respect to the original Shockley state increase linearly with adsorption coverage, thus revealing the importance of the lateral structure of the molecular film in the formation of interface states.

ACKNOWLEDGMENTS

This work has been supported by the Deutsche Forschungsgemeinschaft (DFG) via the Collaborative Research Centre SFB 1083, projects A12 and A13. The authors gratefully acknowledge the computing time granted by the John von Neumann Institute for Computing (NIC) and provided on the supercomputer JUWELS at Jülich Supercomputing Centre (JSC).

[1] M. Rohlfing, R. Temirov, and F. S. Tautz, Adsorption structure and scanning tunneling data of a prototype organic-inorganic interface: PTCDA on Ag(111), Phys. Rev. B **76**, 115421 (2007).

[2] J. Ziroff, F. Forster, A. Schöll, P. Puschnig, and F. Reinert, Hybridization of Organic Molecular Orbitals with Substrate States at Interfaces: PTCDA on Silver, Phys. Rev. Lett. **104**, 233004 (2010).

[3] L. Romaner, D. Nabok, P. Puschnig, E. Zojer, and C. Ambrosch-Draxl, Theoretical study of PTCDA adsorbed on the coinage metal surfaces, Ag(111), Au(111) and Cu(111), New J. Phys. **11**, 053010 (2009).

[4] D. A. Egger, V. G. Ruiz, W. A. Saidi, T. Bučko, A. Tkatchenko, and E. Zojer, Understanding structure and bonding of multilayered metal-organic nanostructures, J. Phys. Chem. C **117**, 3055 (2013).

[5] L. Cao, Y. Wang, T. Chen, W. Zhang, X. Yu, K. Ibrahim, J. Wang, H. Qian, F. Xu, D. Qi, and A. T. S. Wee, Charge transfer dynamics of 3,4,9,10-perylene-tetracarboxylic-dianhydride molecules on Au(111) probed by resonant photoemission spectroscopy, J. Chem. Phys. **135**, 174701 (2011).

[6] T. Ohto, K. Yamashita, and H. Nakamura, First-principles study of electronic structure and charge transport at PTCDA molecular layers on Ag(111) and Al(111) electrodes, Phys. Rev. B **84**, 045417 (2011).

[7] C. Toher, R. Temirov, A. Greuling, F. Pump, M. Kaczmarski, M. Rohlfing, G. Cuniberti, and F. S. Tautz, Electrical transport through a mechanically gated molecular wire, Phys. Rev. B **83**, 155402 (2011).

[8] A. Greuling, M. Rohlfing, R. Temirov, F. S. Tautz, and F. B. Anders, *Ab initio* study of a mechanically gated molecule: From weak to strong correlation, Phys. Rev. B **84**, 125413 (2011).

[9] A Greuling, R. Temirov, B. Lechtenberg, F. B. Anders, M. Rohlfing, and F. S. Tautz, Spectral properties of a molecular wire in the Kondo regime, Phys. Status Solidi B **250**, 2386 (2013).

[10] T. Esat, B. Lechtenberg, T. Deilmann, C. Wagner, P. Krüger, R. Temirov, M. Rohlfing, F. B. Anders, and F. S. Tautz, A chemically driven quantum phase transition in a two-molecule Kondo system, Nat. Phys. **12**, 867 (2016).

[11] R. Temirov, S. Soubatch, A. Luican, and F. S. Tautz, Free-electron-like dispersion in an organic monolayer film on a metal substrate, Nature (London) **444**, 350 (2006).

[12] M. Marks, N. L. Zaitsev, B. Schmidt, C. H. Schwalb, A. Schöll, I. A. Nechaev, P. M. Echenique, E. V. Chulkov, and U. Höfer, Energy shift and wave function overlap of metal-organic interface states, Phys. Rev. B **84**, 081301(R) (2011).

[13] C. H. Schwalb, S. Sachs, M. Marks, A. Schöll, F. Reinert, E. Umbach, and U. Höfer, Electron Lifetime in a Shockley-Type Metal-Organic Interface State, Phys. Rev. Lett. **101**, 146801 (2008).

[14] N. L. Zaitsev, I. A. Nechaev, and E. V. Chulkov, Change in surface states of Ag(111) thin films upon adsorption of a monolayer of PTCDA organic molecules, J. Exp. Theor. Phys. **110**, 114 (2010).

[15] M. S. Dyer and M. Persson, The nature of the observed free-electron-like state in a PTCDA monolayer on Ag(111), New J. Phys. **12**, 063014 (2010).

[16] N. L. Zaitsev, I. A. Nechaev, P. M. Echenique, and E. V. Chulkov, Transformation of the Ag(111) surface state due to molecule-surface interaction with ordered organic molecular monolayers, Phys. Rev. B **85**, 115301 (2012).

[17] M. C. E. Galbraith, M. Marks, R. Tonner, and U. Höfer, Formation of an organic/metal interface state from a Shockley resonance, J. Phys. Chem. Lett. **5**, 50 (2014).

[18] S. S. Tsirkin, N. L. Zaitsev, I. A. Nechaev, R. Tonner, U. Höfer, and E. V. Chulkov, Inelastic decay of electrons in Shockley-type metal-organic interface states, Phys. Rev. B **92**, 235434 (2015).

[19] P. Jakob, N. L. Zaitsev, A. Namgalies, R. Tonner, I. A. Nechaev, F. S. Tautz, U. Höfer, and D. Sánchez-Portal, Adsorption geometry and interface states: Relaxed and compressed phases of NTCDA/Ag(111), Phys. Rev. B **94**, 125436 (2016).

[20] J.-Y. Park, U. D. Ham, S.-J. Kahng, Y. Kuk, K. Miyake, K. Hata, and H. Shigekawa, Modification of surface-state dispersion upon Xe adsorption: A scanning tunneling microscope study, Phys. Rev. B **62**, R16341 (2000).

[21] J. Repp, G. Meyer, and K.-H. Rieder, Snell's Law for Surface Electrons: Refraction of an Electron Gas Imaged in Real Space, Phys. Rev. Lett. **92**, 036803 (2004).

[22] N. Armbrust, F. Schiller, J. Güdde, and U. Höfer, Model potential for the description of metal/organic interface states, Sci. Rep. **7**, 46561 (2017).

[23] A. Sabitova, R. Temirov, and F. S. Tautz, Lateral scattering potential of the PTCDA/Ag(111) interface state, Phys. Rev. B **98**, 205429 (2018).

[24] C. R. Braatz, T. Esat, C. Wagner, R. Temirov, F. S. Tautz, and P. Jakob, Switching orientation of adsorbed molecules: Reverse domino on a metal surface, Surf. Sci. **643**, 98 (2016) (Present challenges in surface science, a special issue in honour of Dietrich Menzel).

[25] F. Bechstedt, *Principles of Surface Physics* (Springer, Berlin, 2003), pp. 114–120.

[26] V. Popescu and A. Zunger, Extracting $\boldsymbol{E}$ versus $\vec{k}$ effective band structure from supercell calculations on alloys and impurities, Phys. Rev. B **85**, 085201 (2012).

[27] C. Lee, Y. Yamada-Takamura, and T. Ozaki, Unfolding method for first-principles LCAO electronic structure calculations, J. Phys.: Condens. Matter **25**, 345501 (2013).

[28] D. Sánchez-Portal, P. Ordejón, E. Artacho, and J. M. Soler, Density-functional method for very large systems with LCAO basis sets, Int. J. Quantum Chem. **65**, 453 (1997).

[29] J. M. Soler, E. Artacho, J. D. Gale, A. García, J. Junquera, P. Ordejón, and D. Sánchez-Portal, The SIESTA method for *ab initio* order-N materials simulation, J. Phys.: Condens. Matter **14**, 2745 (2002).

[30] P. Schröer, P. Krüger, and J. Pollmann, First-principles calculation of the electronic structure of the wurtzite semiconductors ZnO and ZnS, Phys. Rev. B **47**, 6971 (1993).

[31] J. Wieferink, P. Krüger, and J. Pollmann, Improved hybrid algorithm with gaussian basis sets and plane waves: First-principles calculations of ethylene adsorption on β-SiC(001)-(3×2), Phys. Rev. B **74**, 205311 (2006).

[32] B. Stärk, P. Krüger, and J. Pollmann, Magnetic anisotropy of thin Co and Ni films on diamond surfaces, Phys. Rev. B **84**, 195316 (2011).

[33] J. Junquera, Ó. Paz, D. Sánchez-Portal, and E. Artacho, Numerical atomic orbitals for linear-scaling calculations, Phys. Rev. B **64**, 235111 (2001).

[34] D. Sánchez-Portal, E. Artacho, and J. M. Soler, Analysis of atomic orbital basis sets from the projection of plane-wave results, J. Phys.: Condens. Matter **8**, 3859 (1996).

[35] M. J.T. Oliveira and F. Nogueira, Generating relativistic pseudo-potentials with explicit incorporation of semi-core states using APE, the atomic pseudo-potentials engine, Comput. Phys. Commun. **178**, 524 (2008).

[36] A. Tkatchenko and M. Scheffler, Accurate Molecular Van Der Waals Interactions from Ground-State Electron Density and Free-Atom Reference Data, Phys. Rev. Lett. **102**, 073005 (2009).

[37] V. G. Ruiz, Wei Liu, E. Zojer, M. Scheffler, and A. Tkatchenko, Density-Functional Theory with Screened Van Der Waals Interactions for the Modeling of Hybrid Inorganic-Organic Systems, Phys. Rev. Lett. **108**, 146103 (2012).

[38] J. P. Perdew, K. Burke, and M. Ernzerhof, Generalized Gradient Approximation Made Simple, Phys. Rev. Lett. **77**, 3865 (1996).

[39] X. Chu and A. Dalgarno, Linear response time-dependent density functional theory for van der Waals coefficients, J. Chem. Phys. **121**, 4083 (2004).

[40] P. Haas, F. Tran, and P. Blaha, Calculation of the lattice constant of solids with semilocal functionals, Phys. Rev. B **79**, 085104 (2009).

[41] E. Artacho, D. Sánchez-Portal, P. Ordejón, A. García, and J. M. Soler, Linear-scaling *ab-initio* calculations for large and complex systems, Phys. Status Solidi B **215**, 809 (1999).

[42] D. R. Hamann, M. Schlüter, and C. Chiang, Norm-Conserving Pseudopotentials, Phys. Rev. Lett. **43**, 1494 (1979).

[43] L. Kleinman and D. M. Bylander, Efficacious form for Model Pseudopotentials, Phys. Rev. Lett. **48**, 1425 (1982).

[44] We used the decay constants (in atomic units) 0.222, 0.838, and 3.528 for C, 0.315, 1.315, and 5.579 for O, 0.155, 0.681, and 3.531 for H, and 0.230, 0.786, and 2.118 for Ag.

[45] D. M. Ceperley and B. J. Alder, Ground State of the Electron Gas by a Stochastic Method, Phys. Rev. Lett. **45**, 566 (1980).

[46] J. P. Perdew and A. Zunger, Self-interaction correction to density-functional approximations for many-electron systems, Phys. Rev. B **23**, 5048 (1981).

[47] A. W. Maue, Die Oberflächenwellen in der Elektronentheorie der Metalle, Z. Phys. **94**, 717 (1935).

[48] A. Zangwill, *Physics at Surfaces* (Cambridge University Press, Cambridge, 1988), pp. 63–67.

[49] F. Reinert, G. Nicolay, S. Schmidt, D. Ehm, and S. Hüfner, Direct measurements of the l-gap surface states on the (111) face of noble metals by photoelectron spectroscopy, Phys. Rev. B **63**, 115415 (2001).

[50] The reference calculations for the Shockley state of the bare silver surface were carried out including the additional basis orbitals of the adsorbate to avoid basis set errors for the energy shift. This modifies the energy of the Shockley state for the bare silver surface and leads to a small downshift in energy depending on the orbitals of the adsorbate. Therefore, any

adsorbate system has a slightly different reference value for the energy of the Shockley state.

[51] C. Stadler, S. Hansen, A. Schöll, T.-L. Lee, J. Zegenhagen, C. Kumpf, and E. Umbach, Molecular distortion of NTCDA upon adsorption on Ag(111): A normal incidence x-ray standing wave study, New J. Phys. **9**, 50 (2007).

[52] G. Mercurio, R. J. Maurer, W. Liu, S. Hagen, F. Leyssner, P. Tegeder, J. Meyer, A. Tkatchenko, S. Soubatch, K. Reuter, and F. S. Tautz, Quantification of finite-temperature effects on adsorption geometries of π-conjugated molecules: Azobenzene/Ag(111), Phys. Rev. B **88**, 035421 (2013).

[53] J. Li, W.-D. Schneider, and R. Berndt, Local density of states from spectroscopic scanning-tunneling-microscope images: Ag(111), Phys. Rev. B **56**, 7656 (1997).

[54] M. Marks, A. Schöll, and U. Höfer, Formation of metal-organic interface states studied with 2PPE, J. Electron Spectrosc. Relat. Phenom. **195**, 263 (2014).

[55] L. Petersen, P. T. Sprunger, Ph. Hofmann, E. Lægsgaard, B. G. Briner, M. Doering, H.-P. Rust, A. M. Bradshaw, F. Besenbacher, and E. W. Plummer, Direct imaging of the two-dimensional Fermi contour: Fourier-transform STM, Phys. Rev. B **57**, R6858 (1998).

[56] M. F. B. Green, T. Esat, C. Wagner, P. Leinen, A. Grötsch, F. S. Tautz, and R. Temirov, Patterning a hydrogen-bonded molecular monolayer with a hand-controlled scanning probe microscope, Beilstein J. Nanotechnology **5**, 1926 (2014).

[57] P. Leinen, M. F. B. Green, T. Esat, C. Wagner, F. S. Tautz, and R. Temirov, Virtual reality visual feedback for hand-controlled scanning probe microscopy manipulation of single molecules, Beilstein J. Nanotechnology **6**, 2148 (2015).

[58] R. Tonner, P. Rosenow, and P. Jakob, Molecular structure and vibrations of NTCDA monolayers on Ag(111) from density-functional theory and infrared absorption spectroscopy, Phys. Chem. Chem. Phys. **18**, 6316 (2016).

[59] A. Hauschild, R. Temirov, S. Soubatch, O. Bauer, A. Schöll, B. C. C. Cowie, T.-L. Lee, F. S. Tautz, and M. Sokolowski, Normal-incidence x-ray standing-wave determination of the adsorption geometry of PTCDA on Ag(111): Comparison of the ordered room-temperature and disordered low-temperature phases, Phys. Rev. B **81**, 125432 (2010).

[60] K. K. Gomes, W. Mar, W. Ko, F. Guinea, and H. C. Manoharan, Designer Dirac fermions and topological phases in molecular graphene, Nature (London) **483**, 306 (2012).

[61] M. R. Slot, T. S. Gardenier, P. H. Jacobse, G. C. P. van Miert, S. N. Kempkes, S. J. M. Zevenhuizen, C. M. Smith, D. Vanmaekelbergh, and I. Swart, Experimental realization and characterization of an electronic Lieb lattice, Nat. Phys. **13**, 672 (2017).